Increased global heavy fire emission by Madden-Julian Oscillation

Young-Min Yang (ymyang@hawaii.edu)
Nanjing University of Information and science technology https://orcid.org/0000-0002-3048-6430
Doo Young Lee
Pusan National University
Jae-Heung Park
Pohang University of Science and Technology https://orcid.org/0000-0002-8556-2314
June-Yi Lee
Pusan National University https://orcid.org/0000-0002-3986-9753
Soon-Il An
Yonsei University https://orcid.org/0000-0002-0003-429X
Ja-Yeon Moon
4d solution LTd.
Kyung-Sook Yoon
Pusan National University
Tim Li
University of Hawaii at Manoa https://orcid.org/0000-0002-8733-4438
Bin Wang
University of Hawaii at Manoa
Jeong-A Cho
4D solution LTD

Article

Keywords:

Posted Date: January 28th, 2022

DOI: https://doi.org/10.21203/rs.3.rs-1208224/v1

Abstract

Understanding heavy fire activities tied up to climate and its future change is of emerging scientific concern and essential for reducing huge economic costs and life losses from substantial heavy fire hazards under greenhouse warming. Madden-Julian Oscillation (MJO) is a planetary-scale tropical convective system and moves from Asia to the US, generating extreme weather in the midlatitudes. Here, we show that when MJO convective anomalies occur in the western Pacific, the fire emissions in the midlatitudes are two times more likely than when MJO convection is in the Indian ocean. The changes in MJO related to increased fire emissions in the tropics and midlatitudes. Precise MJO predictions may contribute to enhanced subseasonal forecast of the fire activities, aggravating vast social and economic losses (124 words)

Full Text

Fires are a distinct natural disturbance in combustible vegetation areas and release carbons into the atmosphere in a short time scale[1,2]. The emission from fires originated from mid and high latitudes, in particular, is comparable to the fuel emission[3,4]. Hence, to reduce negative social and economic impacts, it is a matter of great importance to investigate dominant factors for generating severe and frequent fires. Fire weather index (FWI)[5] has been used as an indicator of fire potential considering that fire ignition, spread, and frequency can be influenced by specific weather conditions such as temperature, relative humidity, precipitation, and wind speed. It has been suggested that those favorable fire weather conditions can be modulated by human-induced global warming and natural modes of climate variability on interannual to interdecadal timescales[6-11]. The Arctic oscillation and associated jet streams play a role in a fire in the high latitude[12-13], while ENSO affects tropical and mid-latitude fires[11,14]. In a warmer climate, fires are expected to be intensified and occur more frequently with hotter and drier conditions and more lightning occurrences[6-8].

The Madden–Julian oscillation (MJO) is the leading mode of subseasonal variability with 20–100-day periods in the tropics. The MJO is represented by the eastward-propagating deep convective system in the Indian Ocean and western Pacific. The MJO teleconnections have a profound impact on rainfall[15,16,20], drought[19], hurricane[17,18], and regional monsoons[21,22]. The convective heating causes divergent flows in the upper troposphere, generating Rossby wave trains[23-26]. The MJO teleconnection could be a trigger for extreme weather events through generating a heatwave and drying in high-population mid-latitudes, particularly, East Asia, eastern Europe, and United State[23-27]. However, impacts of MJO-related weather conditions on fire occurrences on a global scale are not quantified and remain unresolved. Here we present the relationship between daily fire emission and fire weather conditions regulated by MJO convective anomalies over the eastern Indian Ocean and western Pacific. We bring forward that MJO could be a trigger and booster for fire activities in many tropical and mid-latitude regions by generating severe weather conditions favorable for fires.

Modulation of Fire emission by MJO phase

The strongest FWI anomalies (Fig. 1) occur in the southeast US, central Africa, south Asia, eastern Europe, South America, East Asia. When MJO convection occurs in the western Pacific (MJO phase 5 and 6, hereafter WP phases), FWI in those region is positive, while negative when MJO convection is located at Indian Ocean (MJO phase 2 and 3, hereafter IO phase). Note that in the southern US and Australia, FWI is negative during the WP phase, while positive during the IO phase. The significant symmetric changes of the FWI between WP and IO phase could affect fire emission dominantly. The FWI represents favorable weather conditions for fire activities considering temperature, rainfall, humidity, and wind speed. Thus, it is of particular importance to investigate whether the local FWI anomalies driven by MJO are significantly linked to changes in fire emission or not. The horizontal patterns of fire emission anomalies are consistent with corresponding FWI anomalies at both WP and IP phases (Figure 2). During the WP phase, fire emission in central Africa, South Asia, Eastern Europe, South America, and East Asia is over two or three times than during the IO phase, while fire emission in the southern US and Australia during the WP phase is a half-range value compared to during IO phase. Here we found the new results that the fire emissions in the tropics and midlatitudes are modulated by FWI anomalies generated by MJO atmospheric teleconnection. This is surprising because the fire emission in midlatitudes is intensified or weakened significantly by MJO FWO anomalies and fire emission includes extended-range variability (e.g. sub-seasonal variability). The influence of MJO on fire emission is important because a large portion of MJO-related fire emissions occurs near high population midlatitudes.

Heavy fire emission during MJO events

We want to show whether heavy fire emissions are modulated by MJO or not. Figure 3 shows the histogram of the fire emission and how it has changed over the MJO phase. The results show significant changes in mean fire emission during IO and WP MJO phases. Over East Asia, the mean fire emission during the WP phase is four times more likely than the IO phase. In south Asia, eastern Europe, central Africa, and South America, fire emissions during the WP phase are two times more than IO phase. Note that mean fire emission in the southern US and north Australia during WP is much smaller than that during the IO phase.

We now want to show that fire emissions during the MJO period could be larger than during the normal periods. The horizontal map in figure 4 shows extreme fire emissions corresponding percentile of 95% when data are sorted. The results show that for the same rareness events, the heavy fire emission during MJO period is much larger than the normal period due to the generation of heavy fire-favorable weathers (Supplementary Fig. 1), suggesting that MJO could contribute to generating heavy fire emissions in the tropics and midlatitudes. The frequency of February-April daily fire emission during MJO and all days (Supplementary Fig. 2) over major fire emission regions. The light emission frequency during MJO events is similar to that during all days, while heavy (or extreme) emission frequency during MJO is significantly increased when compared to those during all days over most major fire regions, implying that the MJO teleconnection contributes to the generation of big fire emissions in the mid-latitudes.

The modulation of heavy fire emission by MJO could be verified from recent extreme fire events. August complex fires were extraordinarily large burning in California, 2020. Its size was about 100 km long (north to south) and 50 km wide (east to west). The complex started from 38 separate fires and become one of the largest fires in recorded California history. The complex fire had burned a total of 1million acres, which is about 1% of California's area. Figure 4c shows the temporal evolution of emission and FWI anomalies in the northern California area (39°-40°N, 237°-239°E). During active MJO, two-time series are closely linked to each other. The FWI can capture abrupt peaks of emission anomalies, indicating that the strong emission may have originated from FWI changes induced by the MJO teleconnection. However, during inactive MJO, the changes of both FWI and emission anomalies are relatively small, indicating that MJO teleconnection can contribute to an increase in emission. On the other hand, positive FWI tends to cause the increased emission, while negative FWI is less linked to decreased emission, suggesting that decreased emission may be attributed to other reasons (e.g. human effect). The 2019–20 fire emissions from New South Wales in Australia started early under dry and warm atmospheric conditions. The fires have burned a large portion of the state (55,000 km2). In December 2019, large emission anomalies occurred and moderate emission preceded to late February 2020 (Fig. 4d). Corresponding FWI anomalies reproduce an increase of emission during December 2019 and tend to capture temporal evolution of emission with a correlation of 0.56. These results show that extremely large emissions may be related to the FWI increase induced by MJO teleconnection.

The relationship between fire emission and FWI

This study brings forward that the FWI changes induced by MJO convection should be a key factor in determining the changes in the fire emission, particularly in the mid-latitudes. To further validate this, we compare the relationships between daily FWI and emission anomalies during the active MJO period and total eriods (Fig.5). The results show that the linear relationship between FWI and emission is robust during active MJO periods but very weak during total periods in boreal spring. The relationships between the FWI and emission during total periods are weak with low correlations of 0.17 to 0.34, while they are very strong during active MJO periods with high correlations of 0.58-0.68. The stronger relationship is seen in eastern Europe but weaker in eastern Australia. The strength for the impact of MJO teleconnection (that is, the changes in fire emission by unit change of FWI) depends on the local region and MJO phases. Compared to those during MJO 5 and 6, the strength during MJO 2 and 3 is slightly lower in the southern US, while higher in eastern Australia (Supplementary Fig. 3). On the other hand, there are no significant changes in strength in eastern Asia and eastern Europe.

Contribution of MJO on long-term changes in Fire emission

Previous studies revealed the observed change in MJO residence time[28] and convective activities, which may affect MJO-related decadal changes and trends in fire emission. To assess the potential impacts of the observed changes in the MJO on global fire emission, we calculated the composite difference in fire emission between the 2000s and 2010s (Fig. 6a). The changes in the MJO over the western Pacific are linked with increased fire emission over east Asia, India, the Amazon basin in South America, Central

Africa, and eastern Europe. Meanwhile, the decadal changes in the IO phase are associated with the increases in fire emissions over the southern US and northern Australia (Fig. 6b). Notably, a trend in fire emission for February-April shows consistent changes over most of these regions (Fig. 6c). The increases in mean fire emission are seen in east Asia, India, the Amazon basin, central Africa, central US, and northern Australia. Increased fire emission in the US, East Asia, Northern Australia, and South America may be attributed to an increasing trend in MJO duration. We confirm that composite differences in fire emission with WP and IO MJO phase show similar results as for the trends.

Challenges for enhanced long-range fire emission prediction using MJO forecast

In this study, we present modulation of fire emission and by MJO and the contribution of MJO on heavy emission in the mid-latitude. The fire emission during the WP phase is two times than IO phase. The fire emission data have a significant subseasonal variability in the tropics and midlatitudes (Supplementary Fig. 4). The fire emission associated with MJO teleconnection can explain 10-20% of total emission from subseasonal to interannual variability in the mid-latitude (Supplementary Fig. 5), particularly in the US and East Asia. A recent study suggested that MJO teleconnection will be expected to be amplified in US regions under a warm climate[30], suggesting that the MJO-related fire may be enhanced in the future climate.

The impact of the El Niño event on fire during active MJO periods may be important because the El Nino event changes basic state FWI. In this study, the relatively large decaying El Niño events occurred 2010, 2016, 2019 in boreal spring (Supplementary Fig. 5). During these El Nino years, the MJO-related fire emissions in eastern Europe, East Asia, and eastern Australia are relatively larger than normal years, indicating that the trends in fire emission may be explained at least in part by interaction with El Nino events. The detailed interaction of fire emission with El Nino and MJO will be studied in further study.

The relationship between MJO and fire found in this study could be used for fire prediction. It was known that it takes a few days up to one weeks for Rossby wave excited by MJO convection events to propagate in the mid-latitudes (Supplementary Fig. 6) and a recent state-of-the-art MJO forecast system can predict up to 3-4 weeks in advance[34], suggesting that precise MJO prediction may contribute to improving long-range fire forecast in the midlatitudes, reducing social and economic costs of fires.

Methods

Observed data

For the monthly mean SST, we used the National Oceanic and Atmospheric Administration Extended Reconstructed SST version 5[31]. MJO and its teleconnection are also constructed from two reanalysis datasets: OLR was derived from NOAA satellite data and zonal winds were from the NCEP–DOE reanalysis[32]. Fire weather index (FWI) and geopotential height was obtained from European Center for Medium-Range Weather Forecasts reanalysis v5[33]. Daily outputs, including zonal winds and FWI, were

used. The analysis is conducted for all seasons and covers the same period of fire emission data (2003–2020)

Fire emission data is from the fourth generation of the Global Fire Emissions Database (GFED4, https://www.globalfiredata.org) burned area and emission data set, which provides global monthly, daily, and 3hourly emission data at 0.25° spatial resolution from 2003 to 2020[34].

MJO-related analysis

MJO-related diagnostics. The MJO life cycle is classified by eight MJO phases based on longitudinal locations of the MJO-scale convection. To obtain MJO-phase-composited fields, we calculated daily anomalies and applied a 20-100-days bandpass filter. We also calculated two leading empirical orthogonal functions (EOFs) using the filtered outgoing longwave radiation (OLR), zonal winds at 850hPa, and 200hPa averaged over 10°S-10°N. Using EOFs and filtered OLR and 250hPa and 850hPa zonal winds, we calculated the real-time multivariable MJO (RMM) indices through the projection. The MJO phase 2 and 3 correspond to strong convection over the eastern Indian Ocean, and MJO phase 5 and 6 is characterized by deep convection over the western Pacific. We only select days related to MJO when MJO magnitude is greater than 1. Both concurrent and lag composites were obtained. The Student's t-tests were used to identify where the MJO-phase-composited anomaly is significantly different from zero.

Data Availability

Data related to this paper can be downloaded from the following:

ERSSTv5, https://www.ncdc.noaa.gov/data-access/marineocean-data/extended-reconstructed-sea-surface-temperature-ersst-v5

NOAA/NCEP reanalysis, https://www.esrl.noaa.gov/psd/data/reanalysis/reanalysis.shtml

ECMWF reanalysis, https://www.ecmwf.int/en/forecasts/datasets/browse-reanalysis-datasets

GPCC, https://www.esrl.noaa.gov/psd/data/gridded/data.gpcc.html

All the data generated in this analysis will be deposited at the server clipas.soest.hawaii.edu and are available upon requests.

References

1. Bowman, D. M. et al. Fire in the Earth system. Science 324, 481–484 (2009).
2. Cochrane, M. A. Fire science for rainforests. Nature 421, 913–919 (2003), M. O. & Merlet, P. Emission of trace gases and aerosols from biomass burning. Glob. Biogeochem. Cycles 15, 955–966 (2001).

3. Intergovernmental Panel on Climate Change (IPCC). Climate change 2007: The Physical Science Basis. (Cambridge Univ. Press, 2007).
4. Field, R. D. et al. Development of a Global Fire Weather Database. Nat. Hazards Earth Syst. Sci., 15, 1407–1423 (2015)
5. Flannigan, M. D. & Harrington, J. B. A study of the relation of meteorological variables to monthly provincial area burned by fire in Canada (1953-80). J. Appl. Meteorol. 27, 441–452 (1988).
6. Abatzoglou, J. T. & Kolden, C. A. Relationships between climate and macroscale area burned in the western United States. Int. J. Wildland Fire 22, 1003–1020 (2013).
7. Flannigan, M. D., Logan, K. A., Amiro, B. D., Skinner, W. R. & Stocks, B. J. Future area burned in Canada. Clim. Change 72, 1–16 (2005).
8. Jolly, W., Cochrane, M., Freeborn, P. *et al.* Climate-induced variations in global fire danger from 1979 to 2013. Nat Commun **6**, 7537 (2015). https://doi.org/10.1038/ncomms8537
9. Abatzoglou, J. T. & Williams, A. P. Impact of anthropogenic climate change on fire across western US forests. Proc. Natl Acad. Sci. 113, 11770–11775 (2016)
10. Chen, Y. et al. A pan-tropical cascade of fire driven by El Niño/Southern Oscillation. Nat. Clim. Chang. 7, 906–911 (2017).
11. Wahl, E. R., Zorita, E., Trouet, V. & Taylor, A. H. Jet stream dynamics, hydroclimate, and fire in California from 1600 CE to present. Proc. Natl Acad. Sci. U. S. A. 116, 5393–5398 (2019).
12. Kim, J. S., Kug, J. S., Jeong, S. J., Park, H. & Schaepman, S. G. Extensive fires in southeastern Siberian permafrost linked to preceding Arctic Oscillation. Sci. Adv. 6, eaax3308 (2020).
13. Fang, K., Yao, Q., Guo, Z., Zheng, B., Du, J., Qi, F., et al. (2021). ENSO modulates fire activity in China. Nature Communications, 12(1), 1764. https://doi.org/10.1038/s41467-021-21988-6
14. Wheeler, M. C., Hendon, H. H., Cleland, S., Meinke, H. & Donald, A. Impacts of the Madden–Julian oscillation on Australian rainfall and circulation. J. Clim. 22, 482–1498 (2009).
15. Pohl, B. & Camberlin, P. Influence of the Madden–Julian oscillation on East African rainfall. I: intraseasonal variability and regional dependency. Q. J. R. Meteorol. Soc. 132, 2521–2539 (2006).
16. Maloney, E. D. & Hartmann, D. L. Modulation of eastern North Pacific hurricanes by the Madden–Julian oscillation. J. Clim. 13, 1451–1460 (2000).
17. Klotzbach, P. J. & Oliver, E. C. Modulation of Atlantic basin tropical cyclone activity by the Madden–Julian oscillation (MJO) from 1905 to 2011. J. Clim. 28, 204–217 (2015).
18. Joseph, S., Sahai, A. & Goswami, B. Eastward propagating MJO during boreal summer and Indian monsoon droughts. Clim. Dyn. 32, 1139–1153 (2009).
19. Jia, X., Chen, L., Ren, F. & Li, C. Impacts of the MJO on winter rainfall and circulation in China. Adv. Atmos. Sci. 28, 521–533 (2011).
20. Lorenz, D. J. & Hartmann, D. L. The effect of the MJO on the North American monsoon. J. Clim. 19, 333–343 (2006).

21. Grimm, A. M. Madden–Julian Oscillation impacts on South American summer monsoon season: precipitation anomalies, extreme events, teleconnections, and role in the MJO cycle. Clim. Dyn. 53, 1–26 (2019).
22. Sardeshmukh, P. D. & Hoskins, B. J. The generation of global rotational flow by steady idealized tropical divergence. J. Atmos. Sci. 45, 1228–1251 (1988).
23. Hoskins, B. J. & Karoly, D. J. The steady linear response of a spherical atmosphere to thermal and orographic forcing. J. Atmos. Sci. 38, 1179–1196 (1981).
24. Ferranti, L., Palmer, T. N., Molteni, F. & Klinker, E. Tropical-extratropical interaction associated with the 30–60 day oscillation and its impact on medium and extended range prediction. J. Atmos. Sci. 47, 2177–2199 (1989).
25. Stan, C. et al. Review of tropical-extratropical teleconnections on intraseasonal time scales. Rev. Geophys. 55, 902–937 (2017).
26. . E. National Academies of Sciences, Medicine, Next Generation Earth System Prediction: Strategies for Subseasonal to Seasonal Forecasts. (The National Academies Press, Washington, DC, 2016), pp. 350.
27. Schroeder, W., Oliva, P., Giglio, L., & Csiszar, I. A. (2014). The New VIIRS 375 m active fire detection data product: algorithm description and initial assessment. Remote Sensing of Environment, 143, 85–96. doi: 10.1016/j.rse.2013.12.008 PDF
28. Roxy, M.K., Dasgupta, P., McPhaden, M.J. *et al.* Twofold expansion of the Indo-Pacific warm pool warps the MJO life cycle. Nature **575**, 647–651 (2019). https://doi.org/10.1038/s41586-019-1764-4
29. Maloney, E. D., Adames, Á. F. & Bui, H. X. Madden–Julian oscillation changes under anthropogenic warming. Nat. Clim. Change 9, 26–33 (2019).
30. Zhou, W., Yang, D., Xie, SP. *et al.* Amplified Madden–Julian oscillation impacts in the Pacific–North America region. Nat. Clim. Chang. **10**, 654–660 (2020). https://doi.org/10.1038/s41558-020-0814-0
31. Huang, B. et al. Extended reconstructed sea surface temperature, version 5 (ERSSTv5): upgrades, validations, and intercomparisons. J. Clim. 30, 8179–8205 (2017).
32. Kanamitsu, M. et al. NCEP–DOE AMIP-II Reanalysis (R-2). Bull. Am. Meteorol. Soc. 83, 1631–1644 (2002).
33. ERA5: Fifth Generation Of ECMWF Atmospheric Reanalyses Of The Global Climate (Copernicus Climate Change Service, acessed April 2019); https://doi.org/10.5065/D6X34W69
34. Mariotti, A. et al. Windows of opportunity for skillful forecasts subseasonal to seasonal and beyond. B Am. Meteorol. Soc. 101, E608–E625 (2020).
35. Mu, M., Randerson, J. T., van der Werf, G. R., Giglio, L., Kasibhatla, P., Morton, D., et al. (2011). Daily and 3-hourly variability in global fire emissions and consequences for atmospheric model predictions of carbon monoxide. Journal of Geophysical Research, 116, D24303. https://doi.org/10.1029/2011JD016245

Declarations

Acknowledgments

This work was supported by the National Science Foundation of China (Grant No. 42088101), the National Research Foundation of Korea (NRF; NRF-2018R1A5A1024958 and NRF-2020R1C1C1006569) and Nanjing University of Information Science and Technology initial research foundation (1441012001019). This is Publication No. 11200 of SOEST, Publication No. 1490 of the IPRC, and Publication No. 337 of Earth System Modeling Center.

Author Contributions

Y.-M. Yang, J.-Y. Moon and J.-Y. Lee conceived the idea. Y.-M. Yang, J.-A. Cho and D.-Y. Lee performed analyses. S.-I. An, Y.-M. Yang, Tim Li, B. Wang, and J. H. Park wrote the manuscript. All authors provided critical feedback and helped shape the research, analysis, and manuscript.

Competing Interests statement

The authors declare no competing interests

Supplementary Materials

Supplementary Figure S1-S6

Figures

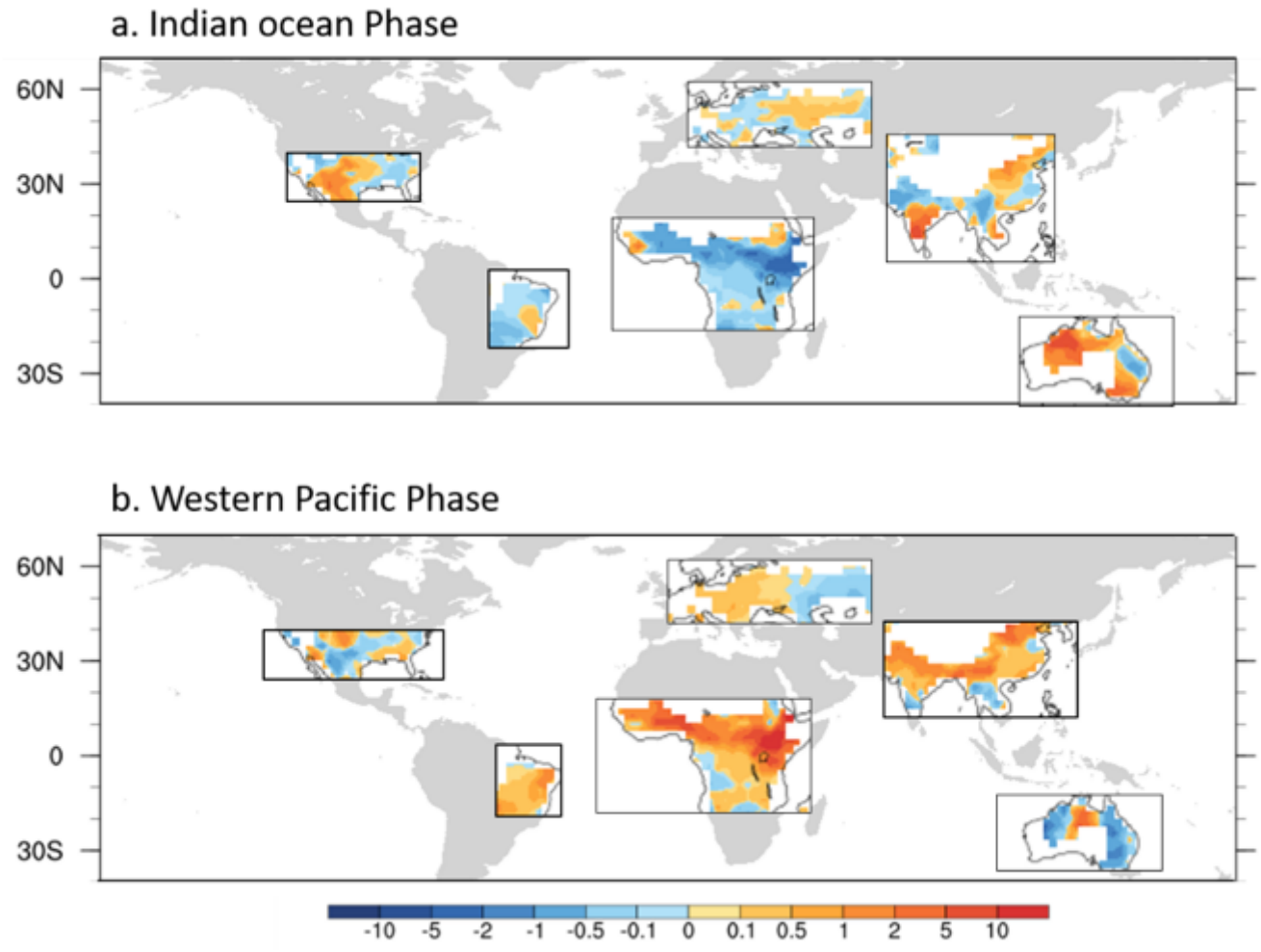

Figure 1

Fire weather index (FWI) during IO and WP phase. a, Composite of February-April FWI during Indian ocean (IO) phase. **b,** same as **a** but during western Pacific (WP) phase. The rectangular box regions indicate large continental areas where the composites in FWI during IO phase are opposite with those during WP phase. 18 years (2003-2020) and 20-100-days bandpass filtered data are used for analysis

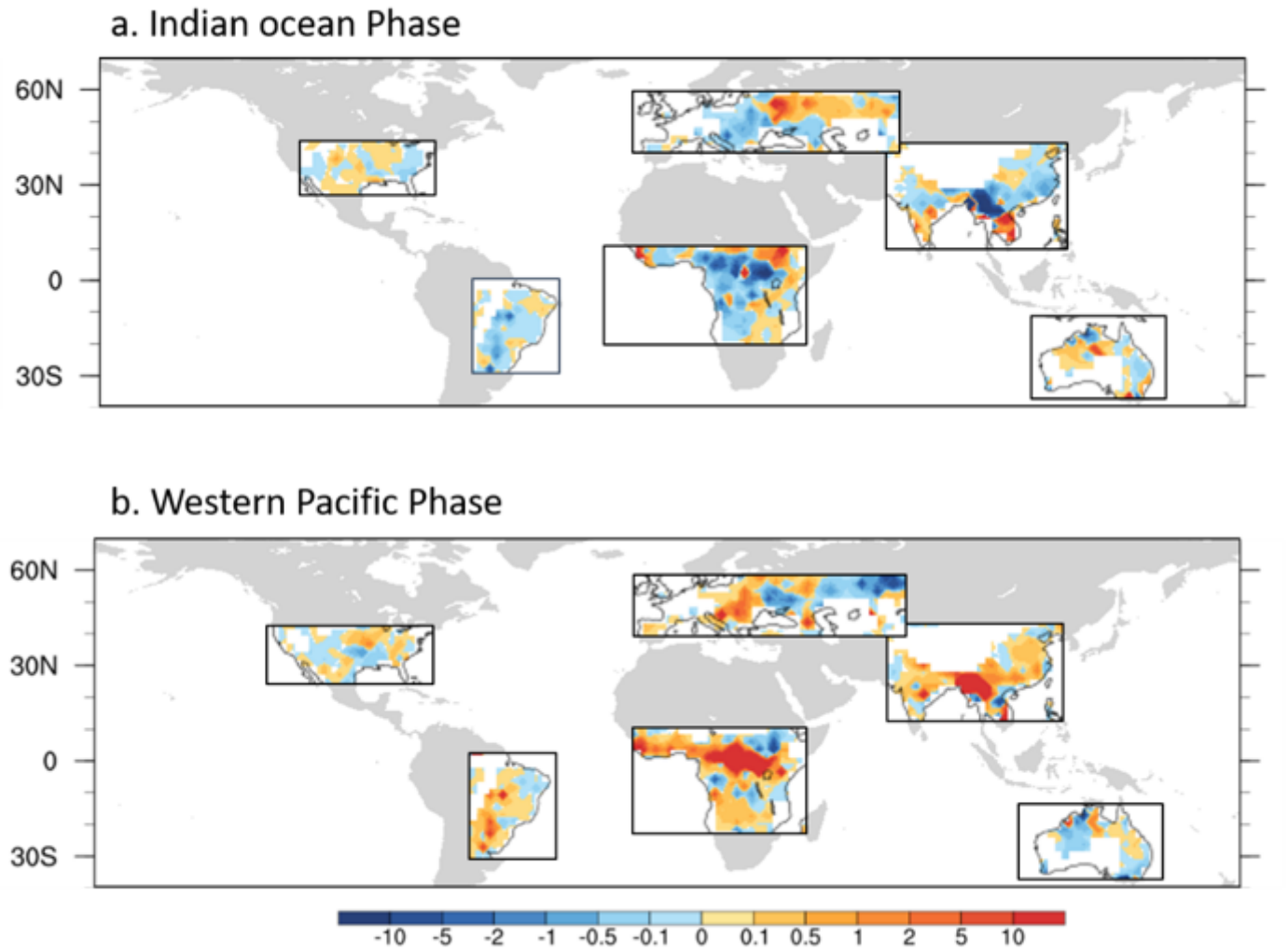

Figure 2

fire emission during IO and WP phase. a, Composite of February-April fire emission anomalies ($\times 10^2$ g C m^{-2} $month^{-1}$) during Indian ocean (IO) phase. **b,** same as **a** but during western Pacific (WP) phase. The rectangular box regions indicate large continental areas where the composite in fire emission during IO phase are opposite with that during WP phase. 18 years (2003-2020) and 20-100-days bandpass filtered data are used for analysis

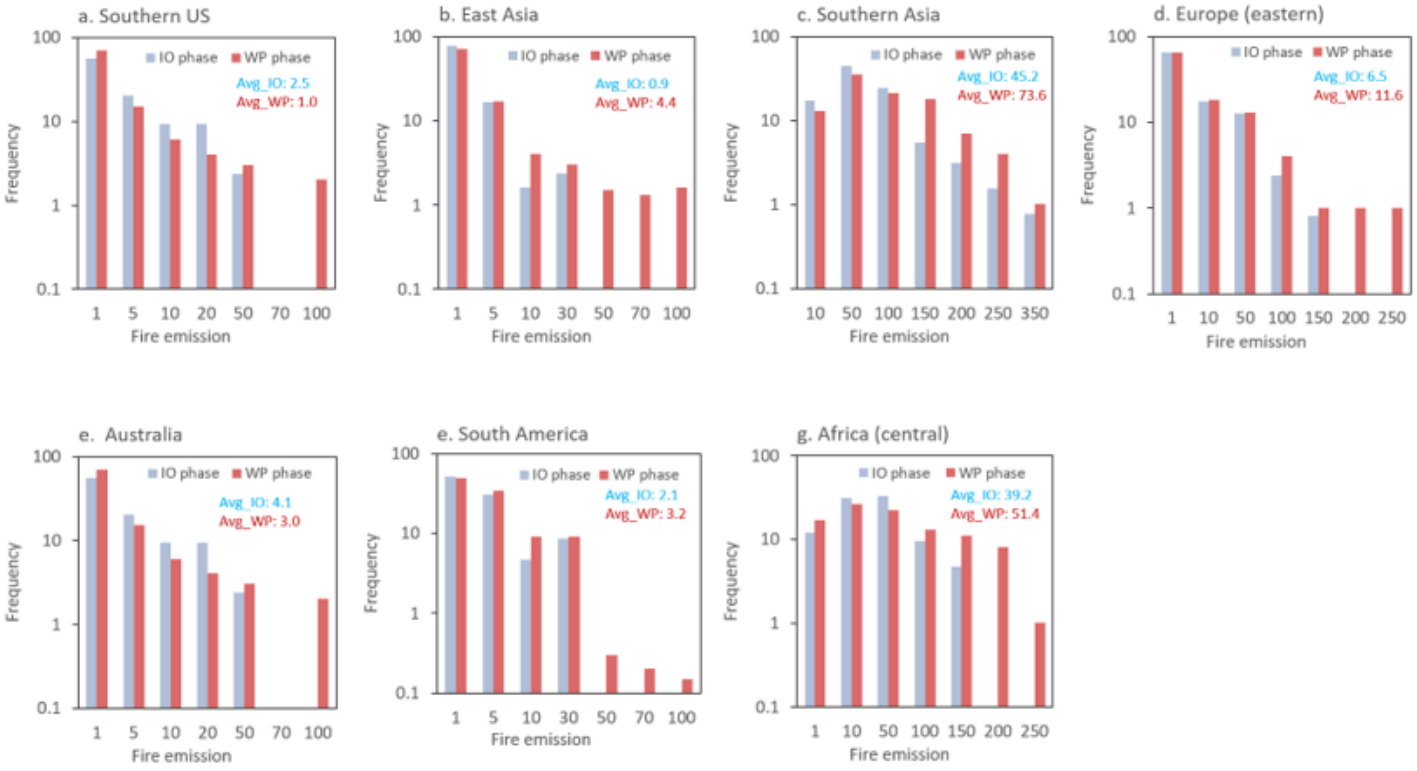

Figure 3

Distribution of fire emission during MJO phase. a-g, Histogram of February-April heavy fire emission ($\times 10^2$ g C m^{-2} $month^{-1}$)) in southern US (a, 31°N-37°N, 260°E-270°E), East Asia (b, 26°N-30°N, 112°E-118°E), south Asia (10°N-20°N, 95°E-110°E), eastern Europe (52°N-58°N, 30°E-40°E), Australia (25S°-15°S, 120°E-130°E), South America (32°S-22°S, 302°E-309°E), and central Africa (0°S-10°N, 22°E-30°E), during IO (light blue bar) and WP (red bar) MJO phase during 2003–2020. The blue (red) number represents the mean fire emission during IO (WP) phase.

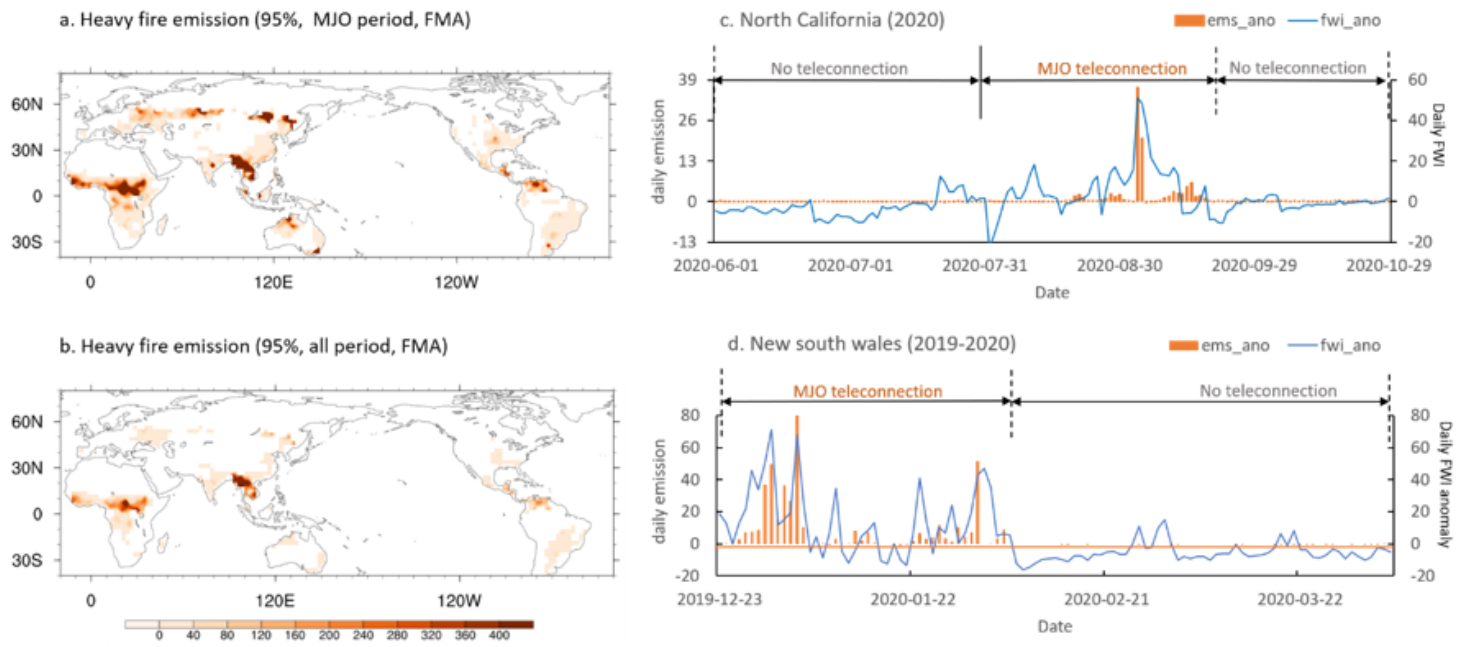

Figure 4

Heavy fire emission during MJO and non-MJO period. a-b, fire emission of 95 % percentile during MJO Period (**a**) and all days (**b**). February-April of 2003-2020 data are used. **c-d,** Temporal evolution of extreme fire emission ($\times 10^2$ g C m^{-2} $month^{-1}$) and corresponding FWI anomalies. Orange bar represent fire emission and blue line shows fire weather index (FWI) anomalies in North California (**c,** 40˚N, 240˚E) at 2020, and southeastern Australia (**d,** 33˚S, 151˚E) at 2020. No filtered data are used.

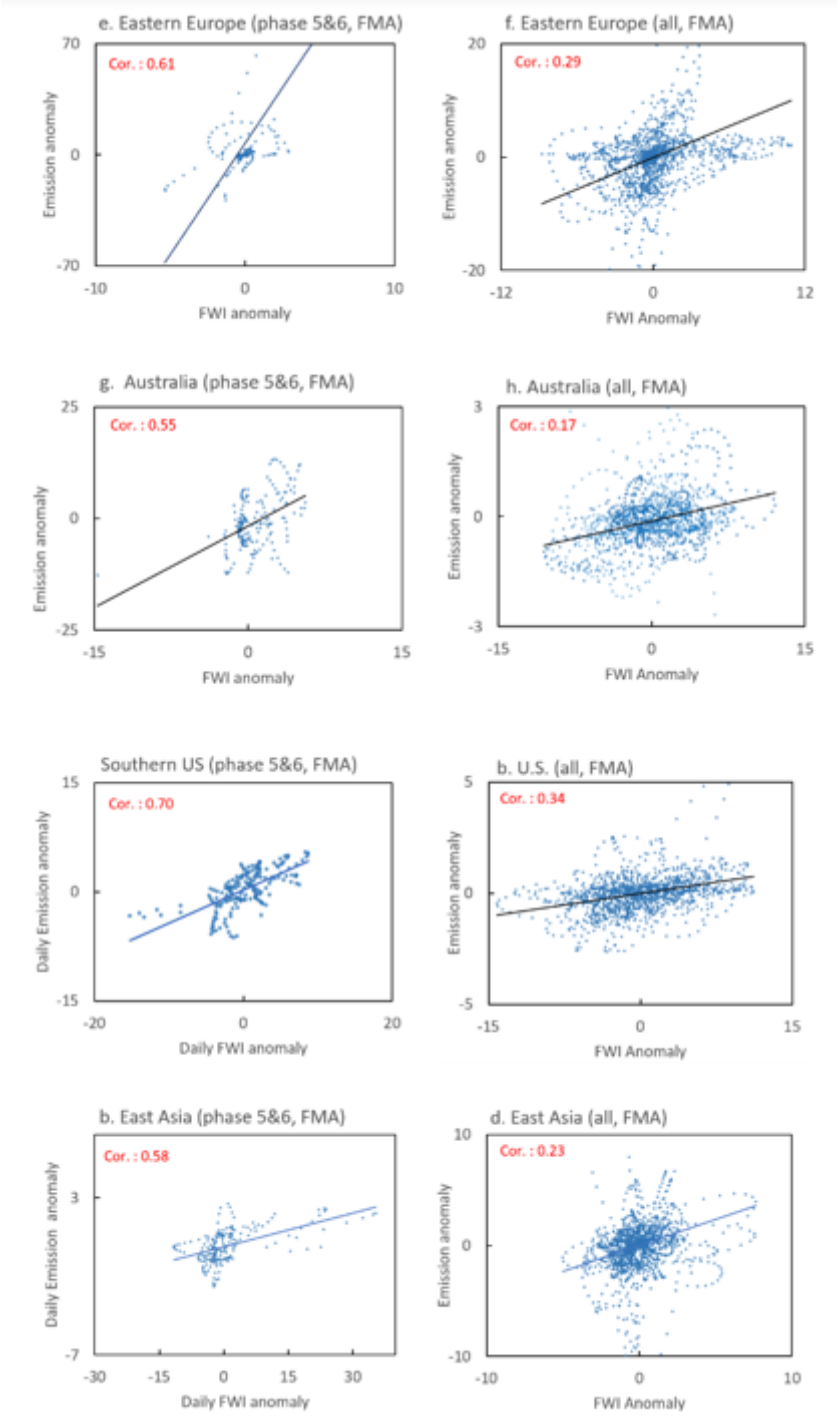

Figure 5

The strong relationship between emission and FWI anomalies. a-b scatter plots of February-April 20-100-days filtered daily fire emission ($\times 10^2$ g C m^{-2} $month^{-1}$) and FWI anomalies in the southern US during MJO phase 2 and 3 (a), and all days (b). c-d same as a-b but for East Asia. e-f same as a-b but for eastern Europe. g-h same as a-b but for eastern Australia. 20-100-day band filtered data for 18 years (2003-2020) are used.

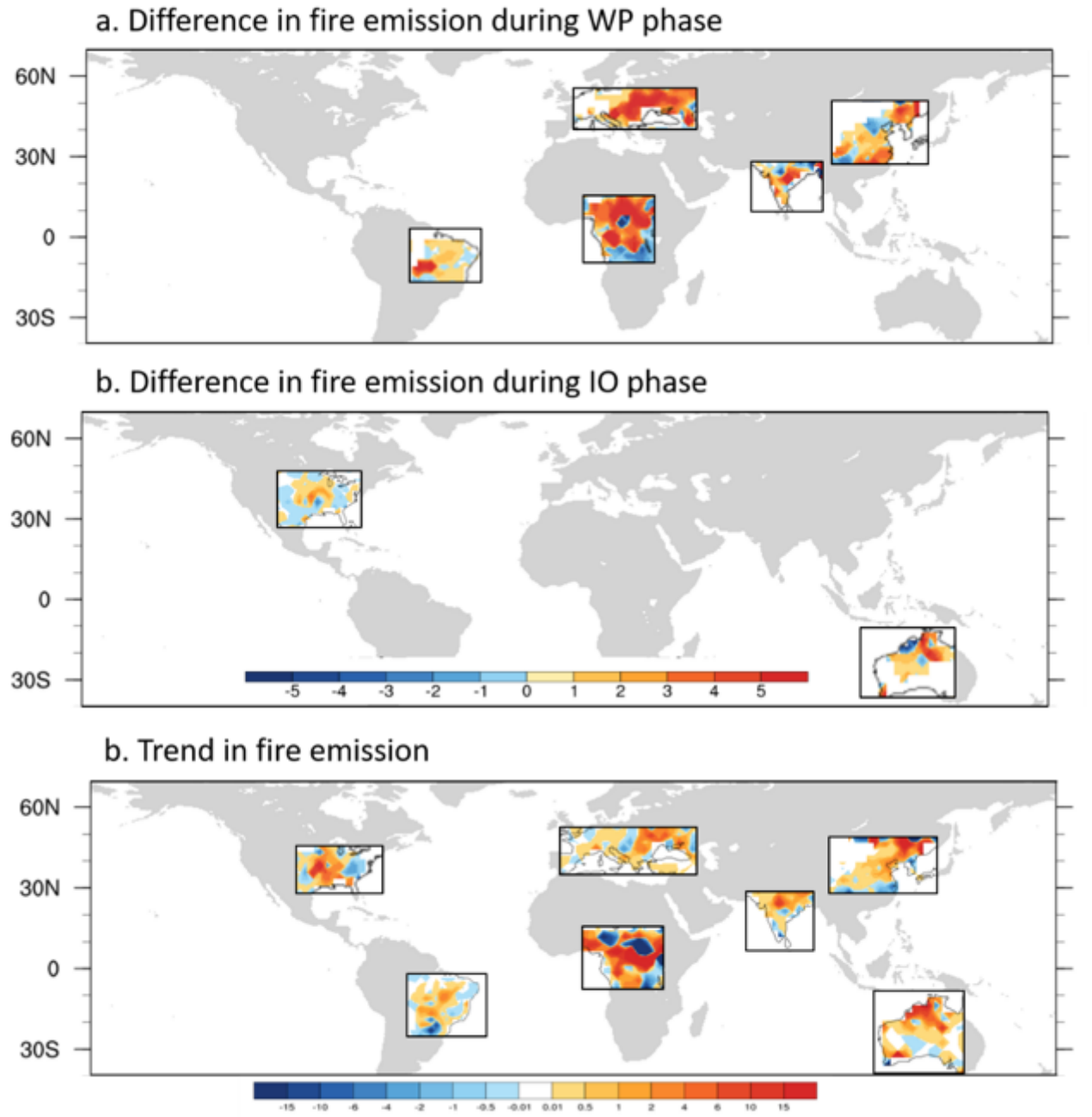

Figure 6

Changes in global fire emission in response to the MJO phase. **a,** Composite difference in February-April fire emission (×10^2 g C m^{-2} $month^{-1}$) between 2003-2010 and 2011-2020 during WP phase. **b,** same as a but during IO phase. **c,** Observed trend in February-April fire emission (×10^2 g C m^{-2} $month^{-1}$) during 2003-2020. The black box regions indicate large continental areas where the trends in fire emission are consistent with the composite analyses.

Supplementary Files

This is a list of supplementary files associated with this preprint. Click to download.

- widfilreMJOsuppv1.3.docx